MOF with Encapsulated CuS Nanoparticles-Based Well-Designed Quercetin Delivery System for Chemo−Photothermal Therapy

Wei Jiang,[†] *Huiyuan Zhang,*[†] *Jilian Wu,*[†] *Guangxi Zhai,*[†] *Zhonghao Li,*[‡] *Yuxia Luan,*[*,†] *and Sanjay Garg*[§]

[†]School of Pharmaceutical Science, Key Laboratory of Chemical Biology, Ministry of Education, Shandong University, Jinan, 250012, China

[‡]Key Lab of Colloid & Interface Chemistry, Shandong University, Ministry of Education, Jinan 250100, China

[§]School of Pharmacy and Medical Sciences, University of South Australia, Adelaide SA 5000

ABSTRACT

Quercetin (QT) is one promising candidate for treatment of various cancers with virtually no toxic side effect. However, its anticancer effect is severely restricted by its poor bioavailability, low water-solubility and chemical instability in the neutral and alkaline medium. Herein, zeolitic imidazolate framework-8 (ZIF-8) is firstly reported as the multi-functional nanoplatform to co-delivery of quercetin as anticancer agent and CuS nanoparticles (NPs) as photothermal therapy (PTT) agent for synergistic combination of chemotherapy and PTT as well as overcoming the drawbacks of quercetin. Moreover, folic acid-bovine serum albumin (FA-BSA) conjugates are

applied to stabilize the CuS@ZIF-8-QT to promote bioavailability of quercetin and realize active targeting drug delivery. Near infrared fluorescent (NIRF) imaging demonstrated the highly increased drug accumulations of FA-BSA/CuS@ZIF-8-QT in tumors, resulting from efficient internalization via FR-mediated endocytosis. The results of *in vivo* and *in vitro* anticancer experiments demonstrate that quercetin and PTT agent can work together efficiently under NIR irradiation, thus remarkably improving anticancer effect. Therefore, our newly designed FA-BSA/CuS@ZIF-8-QT multi-functional drug delivery system might be a promising nanoplatform for cancer treatment.

KEYWORDS: *quercetin, MOF, ZIF-8, chemo-photothermal therapy, targeting, negligible side effect*

1. INTRODUCTION

Cancer is a global public health issue threatening human health seriously, and morbidity of it increases year by year.[1, 2] Among various treatments, chemotherapy is one of the most effective methods. However, most anticancer drugs have severe side effects in clinic, for which the demand for development of new anticancer agents has been raised. Quercetin (3,5,7,30,40-pentahydroxyflavone), one of the most important flavones, is considered as a promising anticancer agent.[3, 4] According to literatures, quercetin can inhibit the proliferation of various cancer cells due to its antioxidant activity and regulation of the expression of tumor suppressor genes metastasis.[5-7]

Notably, quercetin exerts negligible cytotoxicity against normal cells, even at a high level.[8, 9] These properties allowed quercetin served as a promising candidate for treatment of various cancers. However, the anticancer effect of quercetin has been greatly restricted by its poor bioavailability, which is caused by low water-solubility (2.15 μg mL^{-1} at 25 °C)[10] and chemical instability in the neutral and alkaline medium.[11] For the use of quercetin in the antitumor fields, a rational drug delivery system is highly on demand.

Recently, metal organic frameworks (MOFs) have been investigated as a drug carrier owing to their regular porosity, high pore volume, easy surface-functionalization, excellent thermal and chemical stability.[12-14] Among others, zeolitic imidazolate framework-8 (ZIF-8), a biocompatible MOF constructed of zinc ions and 2-methylimidazolate, is a promising drug delivery vehicle because it has good stability under physiological conditions, while disintegrating at tumor site due to extracellular lower pH value.[15-17] Due to the opposite charges and coordination effect between quercetin and ZIF-8, we hypothesized that quercetin could be loaded into the ZIF-8 matrix with high loading capacity.

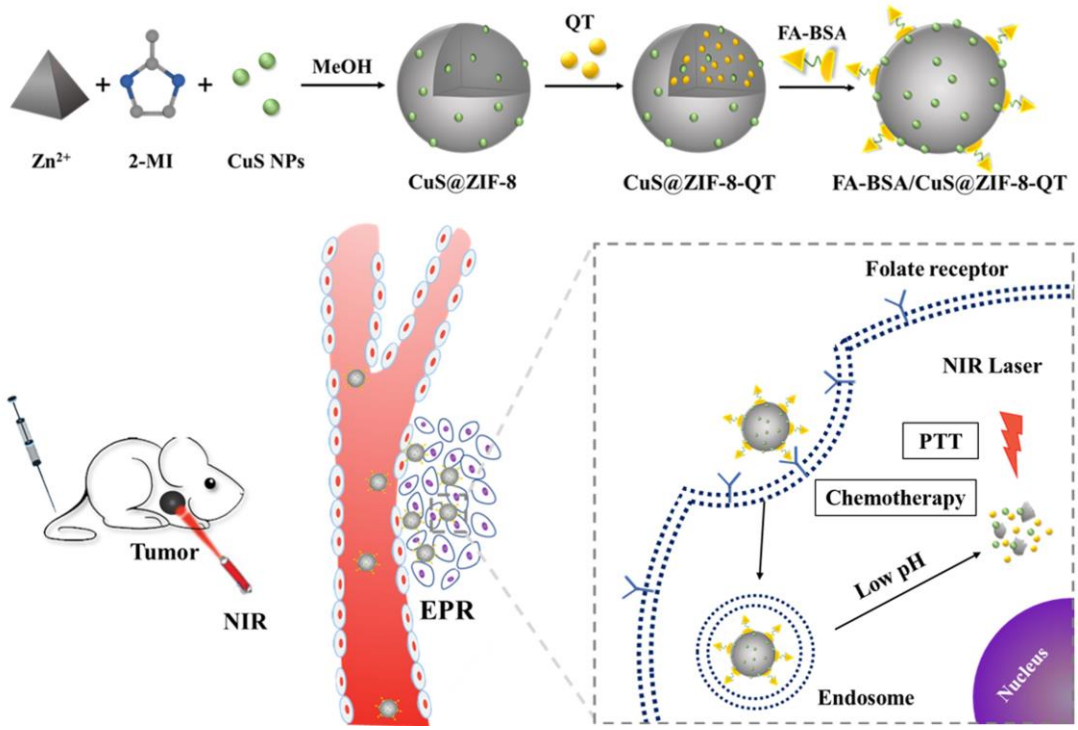
Photothermal therapy (PTT) that exploits light (most often in infrared wavelengths) induced hyperthermia to kill the targeted cells, is an efficient cancer therapy method, featuring noninvasiveness, safety, and efficiency compared with traditional cancer treatments (including chemotherapy, radiotherapy and surgery).[18-20] Recently, much effort has been made to construct composite nanoparticles as chemo-photothermal therapy platforms to enhance the therapeutic efficacy and to decrease the

multidrug-resistance of cancer cells.[21-24] Considering the variability and complexity of cancers and the insufficient anticancer effect of quercetin, we attempt to introduce PTT into our drug delivery system in this work. CuS NPs, one of the most common PTT agents in the nanocomposites for chemo-photothermal therapy,[25-28] have also been reported to encapsulate in the framework of ZIF-8 without obvious influencing the drug load or altering its pH-sensitive property.[29] Inspired by this, herein, the anticancer drug quercetin and PTT agent CuS NPs are integrated into one system, enabling synergistic combination of chemotherapy and PTT.

Bovine serum albumin (BSA), with good adhesiveness to solid surfaces due to hydrophobic and hydrophilic patches on their surfaces, is widely used in drug delivery system as a stabilizer or reductant.[30] Moreover, quercetin can bind with BSA through hydrophobic interaction and hydrogen bond according to reports.[31-33] Therefore, BSA can be used as both a reductant and a stabilizer to promote solubility, stability and bioavailability of quercetin.[34] Folate is one of the most common targeting ligand, grafted with which nanocarriers can specifically transport anticancer drugs to tumors via targeting effect of the folate to overexpressed FA-receptors (FR) on the tumor cells. In addition, FA-BSA conjugation is a satisfactory stabilizer and target agent according to our previous studies.[35, 36] Therefore, FA-BSA can serve as promising stabilizers for nanocarriers to overcome the drawback of quercetin and achieve targeting drug delivery.

Herein, we proposed a pH-responsive, FA-BSA functionalized hybrid MOF nanoplatform (FA-BSA/CuS@ZIF-8-QT) for cancer therapy, which can achieve

satisfactory drug loading, overcome the drawbacks of quercetin, improve drug delivery and cellular uptake, fulfill synergistic combination of chemotherapy and PTT, and finally enhance antitumor effect. The synthesis procedure of the FA-BSA/CuS@ZIF-8-QT NPs is shown in Scheme 1. CuS NPs were obtained by hydrothermal synthesis, in which PVP was used as the growth template and stabilizing agent. When 2-methylimidazole (2-MI) mixed with the PVP-modified CuS NPs in solution, more 2-MI molecules gathered around CuS NPs due to the hydrogen bond between 2-MI and PVP, so ZIF-8 would grow around CuS NPs to form the CuS@ZIF-8 NPs with the addition of Zn^{2+}. Then the quercetin loading was performed by introducing via chelation and electrostatic interactions. Finally, FA-BSA conjugate was synthesized via amide bond as targeting agent which attached to the surface of the drug-loading MOF by interaction between protein and nanoparticles. After intravenous injection, the as-prepared nanoparticles accumulate at tumor tissues and then are efficiently taken up by cancer cells via FR-mediated endocytosis. With the release of quercetin, tumor site is exposed to NIR to realize the combination of chemotherapy and PTT. In this study, the efficient pH-responsive and NIR-induced drug release behavior, excellent photothermal effect, enhanced cellular uptake, synergistic anticancer efficacy of quercetin and PTT *in vitro* and *in vivo* of FA-BSA/CuS@ZIF-8-QT NPs had been verified, demonstrating that our designed drug delivery system could take full advantage of quercetin for the effective cancer therapy.



Scheme 1. Schematic illustration of the combinational therapy platform based on FA-BSA modified ZIF-8 (FA-BSA/CuS@ZIF-8-QT).

2. EXPERIMENTAL SECTION

2.1. Materials. Quercetin dihydrate (QT, > 96.0%), 2-methylimidazole (2-MI) and zinc nitrate hexahydrate ($Zn(NO_3)_2 \cdot 6H_2O$, AR) were purchased from Beijing J & K Technology Co., Ltd. Copper (II) chloride dihydrate ($CuCl_2 \cdot 2H_2O$), sodium sulfide (Na_2S) and polyvinylpyrrolidone (PVP-k30, 40 KDa) were supplied by Shanghai Aladdin Bio-Chem Technology Co., Ltd. Folic acid (FA) was supplied by Sigma Co. Ltd. Bovine serum albumin (BSA) was supplied by Beijing Dingguo Changsheng Biotech. Co., Ltd. 3-(4,5-dimethylthiazol-2-yl)-2,5-diphenyltetrazolium bromide (MTT) was supplied by Beijing Solarbio Technology Co., Ltd. IR820 was purchased from Suzhou BEC Biological Technology Co., Ltd. Annexin V-FITC/propidium

iodide (PI) apoptosis detection kit was supplied by Yeasen Biotech Co., Ltd. (Shanghai, China).

2.2. Synthesis of CuS@ZIF-8. The preparation of PVP-modified CuS NPs refers to a previous report.[29] Then, 8 mL as-prepared CuS NPs methanol solution (1.0 mg mL^{-1}) was mixed with 12 mL of 2-methylimidazole methanol solution (649 mg, 7.90 mmol). After being stirred for 30 min, the above mixture was added with 20 mL of $Zn(NO_3)_2 \cdot 6H_2O$ methanol solution (293 mg, 0.98 mmol), then stirred for another 1 h. Afterward, CuS@ZIF-8 NPs obtained by centrifugation (14000 rpm, 15 min) was washed twice by methanol, then re-dispersed in 4 mL methanol. All the above processes were conducted at room temperature.

2.3. Quercetin Loading. The above CuS@ZIF-8 methanol solution was mixed with 36 mL of quercetin methanol solution (6 mg mL^{-1}), then the mixture was stirred for 24 h. CuS@ZIF-8-QT NPs were collected by centrifugation (14000 rpm, 15min), then washed twice by methanol and twice by deionized water. Finally, tawny powders after lyophilization were obtained.

2.4. Preparation of FA-BSA/CuS@ZIF-8-QT. FA-BSA/CuS@ZIF-8-QT was prepared by surface modification of CuS@ZIF-8-QT with FA-BSA. The synthesis of FA-BSA was according to our previous report.[35,36] As demonstrated by UV−vis spectra (Figure S1), the FA-BSA was successfully synthesized. CuS@ZIF-8-QT NPs was dispersed in 5 mL of FA-BSA alkali aqueous solution and further stirred for 30 min. And then FA-BSA/CuS@ZIF-8-QT NPs were collected by centrifugation, washed twice by deionized water. Finally, tawny powders after lyophilization were

obtained.

2.5. Characterization. The Fourier transform infrared (FTIR) analysis was carried on by a FTIR Spectrometer (Thermo Fisher Scientific, Nicolet 6700). The morphologies of the nanoparticles at each preparation step was characterized by transmission electron microscope (TEM, JEM-200 CX). The particle sizes were measured by dynamic light scattering (DLS, Brookhaven BI-200SM). Scanning electron microscopy (SEM) was conducted by a FESEM (Hitachi, SU-70). The UV−vis-NIR spectra were measured by a UV−vis spectrophotometer (Metash, UV-8000). Zeta potential was determined by Zetasizer Nano ZS90 (Malvern).

2.6. Stability study of quercetin in formulations. Free quercetin, CuS@ZIF-8 and FA-BSA/CuS@ZIF-8 were dispersed in deionized water respectively to obtain aqueous dispersions with same quercetin concentration. At each predetermined time, 0.5 mL of each samples were collected and treated with 0.5 mL diluted hydrochloric acid to disintegrate carriers, and then diluted with methanol to dissolved quercetin completely. Afterwards the absorbance of the solution at 370 nm was measured. The relative intensity was calculated as follows:

$$\text{Relative intensity} = (A_{sample} - A_{positive}) / (A_{negative} - A_{positive})$$

Where $A_{positive}$ and $A_{negative}$ represents the absorbance of the quercetin dispersed in deionized water for 72 h and 0 h, respectively.

2.7. Photothermal Effect of FA-BSA/CuS@ZIF-8-QT NPs. The photothermal effects of FA-BSA/CuS@ZIF-8-QT were determined by using an 808 nm laser (MW-GX-808/10W, spot size: 6 mm, power density: 2 W cm^{-2}). Samples of different

CuS concentrations in 24-well plates were irradiated by 808 nm laser with a digital thermometer monitoring the temperature changes of the solutions. And the photothermal images were taken by a thermal camera (FLUKE, Testo 869).

2.8. *In Vitro* Drug Release of FA-BSA/CuS@ZIF-8-QT. To determine the pH responsibility of the drug-loaded ZIF-8 as well as evaluate effect of NIR on it, dialysis method was used to investigate the *in vitro* release behavior. Dialysis bags (MWCO = 3500) containing 1 mL of FA-BSA/CuS@ZIF-8-QT aqueous dispersions were put into the phosphate buffer saline (PBS containing 1% Tween 80, pH = 7.4 and 5.0) at 37 ± 1.0 °C with continuous sharking (100 rpm). After 3 h incubation, dialysis bags of NIR groups were exposed to an 808 nm laser (2 W cm^{-2}, 5 min). At each predetermined time, 2 mL of the release medium were taken out with supplement of 2 mL fresh medium. The content of quercetin in the release medium was determined by UV-vis spectrophotometer. And the release experiments at all conditions were performed three times in parallel.

2.9. Hemolysis Assay. Hemolysis assay was performed to evaluate the feasibility of the FA-BSA/CuS@ZIF-8-QT for intravenous administration. Whole blood samples obtained from New Zealand white rabbit were washed and diluted with normal saline to prepare 2% (V/V) red blood cells suspension. The sample groups were composed of 1.25 mL RBC, 1.1 mL NS and 0.15 mL formulation (CuS NPs, CuS@ZIF-8 and FA-BSA/CuS@ZIF-8-QT) in different concentrations. Negative and positive control groups were obtained by adding 1.25 mL RBC into 1.25 mL NS or distilled water respectively. After 3 h thermostatic incubation (37.0 ± 1.0 °C), all samples were

centrifugated (1500 rpm, 15 min). Then the UV-vis absorbance at 540 nm of the supernatant was measured. Each group was measured three times in parallel. The hemolysis ratio was calculated as follows:

$$\text{Hemolysis (\%)} = (A_{sample} - A_{negative}) / (A_{positive} - A_{negative}) \times 100$$

Where $A_{negative}$, $A_{positive}$ and A_{sample} represent the UV−vis absorbance of negative control group, negative control group, and formulation groups, separately.

2.10. Cell Culture. The cell experiments were carried out on B16F10 cells (a cell line of mouse melanoma cells). The cells were cultured with the 1640 culture medium containing 10% FBS and 1% penicillin-streptomycin in incubator (37 °C, 5.0% CO_2).

2.11. *In Vitro* Cytotoxicity Studies. The photothermal efficiency and *in vitro* anticancer efficacy of FA-BSA/CuS@ZIF-8-QT against B16F10 cells were studied by MTT method. CuS@ZIF-8-QT and free quercetin were used as controls. First, B16F10 cells were cultured in 96-well plates (5×10^3 cells/well) and incubated overnight. Then, culture medium was replaced with fresh cell medium containing serial dilutions of different formulations (FA-BSA/CuS@ZIF-8-QT nanoparticles, CuS@ZIF-8-QT, free quercetin from 10 to 150 μM of quercetin). For laser groups, 808 nm laser (2 W cm^{-2}, 5 min) were performed to irradiate the cells incubated with formulations for 4 h. After another 20 hours incubation, 10 μL 5% MTT were added to the medium then cells were incubated at 37 °C for 4 h. Subsequently, the medium was replaced with 150 μL DMSO to dissolve generated formazan crystals. After that, a microplate reader (ELIASA of PerkinElmer) was used to measure the absorbance at 490 nm. All groups were repeated thrice. The cell inhibition rate was counted by the

following equation:

$$\text{Cell inhibition rate (\%)} = (A_{positive} - A_{sample}) / (A_{positive} - A_{blank}) \times 100$$

Where $A_{positive}$, A_{blank} and A_{sample} represent absorbance of the positive control group (pure culture media), blank control group (culture medium without cells or drugs) and sample group, respectively.

2.12. *In Vitro* Cellular Uptake Assay. Fluorescence inverted microscope (ECLIPSE-Ti, Nikon) and flow cytometry were used to investigate the *in vitro* cell uptake ability of FA-BSA/CuS@ZIF-8-QT. IR820, as a fluorescence probe marking the vehicle, [37, 38] replaced the drug to carry out the assay. The preparation procedure of FA-BSA/CuS@ZIF-8-IR820 was similar to FA-BSA/CuS@ZIF-8-QT. Briefly, B16F10 cells were cultured in 6-well plates (2×10^5 cells/well) and incubated overnight. Then the medium was replaced with 2 mL fresh cell medium containing different formulations (FA-BSA/CuS@ZIF-8-IR820, CuS@ZIF-8-IR820, or free IR820, with the IR820 concentration of 20 μg mL^{-1}). After internalization of formulations for 4 h, medium was removed and cells were washed with PBS thrice. Then the cellular uptake behavior of samples was observed and photographed by fluorescent inverted microscope. Further quantitatively analyze was performed by flow cytometry (BD FACSAria III). All cells samples were collected after washed with PBS twice, then dispersed in PBS for flow cytometry analysis.

2.13. Cell Apoptosis Assay. For cell apoptosis assay, B16F10 cells were cultured in 6-well plates (5×10^5 cells/well) and treated with (1) control; (2) NIR; (3) free quercetin (100 μM); (4) CuS@ZIF-8-QT (100 μM of QT); (5)

FA-BSA/CuS@ZIF-8-QT (100 μM of QT); (6) CuS@ZIF-8 + NIR (100 μM of Cu^{2+}); (7) CuS@ZIF-8-QT + NIR and (8) FA-BSA/CuS@ZIF-8-QT + NIR (100 μM of QT) for 4 h. For NIR-related groups, cells were irradiated with NIR (808 nm, 2 W cm^{-2}) for 5 min after washed with PBS. Subsequently, all cells samples were collected after washed with cold PBS twice, then stained by the annexin V-FITC/PI apoptosis assay kit combined with further characterization by flow cytometry (BD FACSAria III).

2.14. Establishment of Animal Melanoma Models. All animal experiments complied with the stipulation of the Institution Animal Care. Healthy male BALB/C mice (2-3 weeks) were supplied by Shandong University laboratory animal center. 0.1 mL PBS suspension containing 1.5 × 10^6 B16F10 cells was subcutaneously injected into mice's right anterior armpit.

2.15. *In Vivo* NIRF Imaging. The mice bearing B16F10 tumor (~150 mm^3) were divided into two groups randomly (n = 5). Two groups of mice were injected with CuS@ZIF-8-IR820 or FA-BSA/CuS@ZIF-8-IR820 (IR820 concentration: 1.5 mg kg^{-1}) through caudal vein respectively. At each predetermined time point, fluorescent images of anaesthetized mice were collected by the *in vivo* imaging systems (Xenogen IVIS Kinetic system). At the end of the study, those mice were dissected. Then main organs and tumors were collected for the measurements of their fluorescence intensity.

2.16. *In Vivo* Infrared Thermography and Anti-Tumor Efficacy Assay. The mice bearing B16F10 tumor (~150 mm^3) were divided into four groups randomly (n = 5). Each group were intravenously injected with (1) saline, (2) free quercetin, (3)

CuS@ZIF-8-QT, (4) FA-BSA/CuS@ZIF-8-QT (QT dose: 10 mg kg^{-1}, CuS dose: 3 mg kg^{-1}) every 3 days, respectively. At 8 h postinjection, the tumor sites of all mice were exposed to NIR (808 nm, 1 W cm^{-2}, 5 min) with a thermal camera (FLUKE, Testo 869) to recorded the temperature change. Every 2 days in this study, mice's tumor volume and body weight were measured and recorded. Tumor volume (V) was obtained by the following formula: $V = L \times W^2 / 2$, in which W and L represented shortest and longest diameter of tumor.[39] Tumor inhibition ratio was calculated as follows:

$$\text{Tumor inhibition ratio (\%)} = (1 - W_t / W_c) \times 100$$

Where W_c and W_t represent the average tumor weight of control groups and treatment group, separately.

2.17 Survival Study. The mice bearing B16F10 tumor (~300 mm^3) were divided into two groups (n = 12). Treatment group were injected with FA-BSA/CuS@ZIF-8-QT (QT dose: 10 mg kg^{-1}) through tail vein and the tumor sites were irradiated with NIR (808 nm, 1 W cm^{-2}) for 5 min at 8 h postinjection, while control group were intravenously injected with normal saline. The above treatments were carried out every three days and the mortality of the mice was monitored every day.

2.18. Histology Analysis. Mice were dissected after the anti-tumor efficacy assay. Their tumors and main organs were harvested and then fixed by 4% formalin for further tissue sections making. After stained by hematoxylin and eosin (HE), tissue sections were characterized and photographed by NIKON Eclipse Ci light microscope.

3. Results and Discussion

3.1. Preparation and Characterization of FA-BSA/CuS@ZIF-8-QT NPs. The synthesis procedure of the FA-BSA/CuS@ZIF-8-QT NPs was shown in Scheme 1. The Fourier transform infrared (FTIR) spectra of ZIF-8, CuS@ZIF-8, CuS@ZIF-8-QT and FA-BSA/CuS@ZIF-8-QT were shown in Figure 1A. Compared with ZIF-8, the new peaks at 1671 cm^{-1} in the FTIR spectrum of CuS@ZIF-8 can be assigned to the C=O stretching bond vibration of PVP in the CuS NPs, which demonstrated that CuS NPs successfully encapsulated in the framework of ZIF-8. The new peaks at 1639 cm^{-1} and 3138 cm^{-1} in the FTIR spectrum of CuS@ZIF-8-QT can be assigned to the stretching vibration of O–H and C-H in benzene, respectively, confirming that quercetin was loaded into the CuS@ZIF-8. In the FTIR spectrum of FA-BSA/CuS@ZIF-8-QT, the stretching vibration peak of C-N and amide II absorption of the N-H bond characteristic peak appeared at 1425 cm^{-1} and 1579 cm^{-1}, demonstrating that the FA-BSA conjugate successful attached to the surface of the CuS@ZIF-8-QT. Figure 2B showed the UV-vis-NIR spectra of CuS NPS, ZIF-8 and CuS@ZIF-8 nanocomposites. The aqueous dispersion of ZIF-8 nanoparticles exhibited no obvious absorption in the ranging from 700 to 1100 nm, while CuS NPs showed a broad absorption band which also existed in the spectrum of CuS@ZIF-8, further confirming that the successfully preparation of CuS@ZIF-8.

The transmission electron microscope (TEM) images of ZIF-8, CuS@ZIF-8-QT and FA-BSA/CuS@ZIF-8-QT in Figure 1C demonstrated that both formulations

(CuS@ZIF-8-QT NPs and FA-BSA/CuS@ZIF-8-QT NPs) exhibited uniform spherical-like morphology with about 30 nm. In addition, compared with smooth surfaces of ZIF-8 NPs, there were several small particles on the surfaces of CuS@ZIF-8-QT NPs and FA-BSA/CuS@ZIF-8-QT NPs, indicating they were composed of two parts: ZIF-8 framework and embedded CuS NPs. The elemental mapping results (Figure S2, Supporting Information) also verified that the CuS NPs were embedded into the ZIF-8. The dynamic light scattering (DLS) analysis indicated that the particle sizes of ZIF-8 NPs, CuS@ZIF-8-QT NPs and FA-BSA/CuS@ZIF-8-QT NPs were 32.5 ± 13.1 nm, 37.4 ± 11.4 nm, 45.1 ± 15.0 nm respectively (Figure. 1D), which were approximately in agreement with the TEM results. The FA-BSA/CuS@ZIF-8-QT NPs have larger size than CuS@ZIF-8-QT NPs, demonstrating its successful modification of FA-BSA. As shown in Figure S3, the zeta potentials of ZIF-8, CuS@ZIF-8, CuS@ZIF-8-QT and FA-BSA/CuS@ZIF-8-QT were 32.8 ± 7.4 mV, 26.7 ± 6.2 mV, −23.6 ± 6.6 mV, and -27.9 ± 6.0 mV respectively. The zeta potential variation agrees well with the negative charge characteristic of QT and FA-BSA.

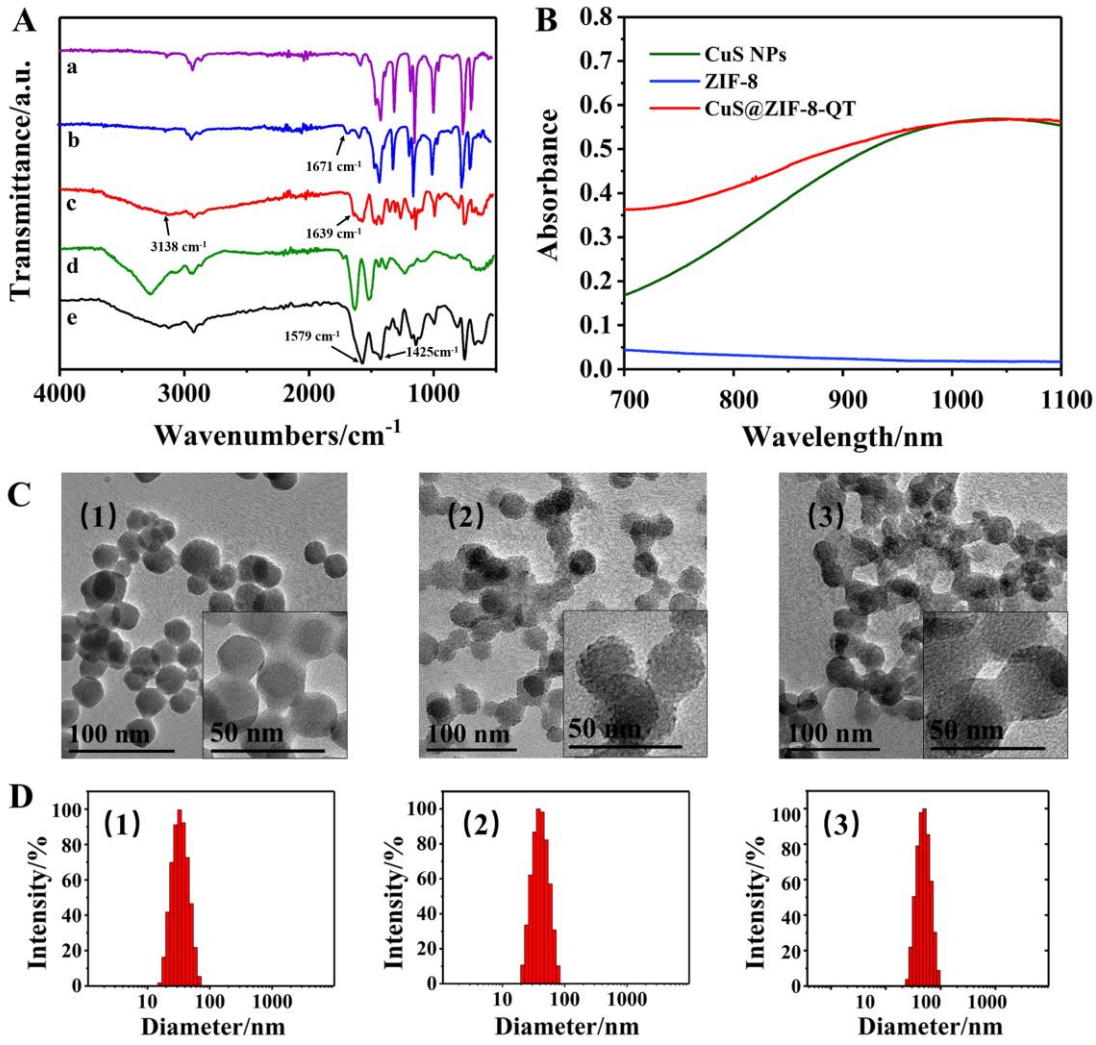


Figure 1. A) FTIR spectra of (a) ZIF-8 (a), (b) CuS@ZIF-8, (c) CuS@ZIF-8-QT, (d) FA-BSA and (e) FA-BSA/CuS@ZIF-8-QT. B) UV–vis-NIR spectra of CuS@ZIF-8 and corresponding CuS NPs and ZIF-8. C) TEM images and D) size distributions of (1) ZIF-8, (2) CuS@ZIF-8, (3) FA-BSA/CuS@ZIF-8-QT.

To evaluate the stability of quercetin in the samples of free quercetin, CuS@ZIF-8-QT and FA-BSA/CuS@ZIF-8-QT, the variations in the relative intensities of the characteristic UV absorbance peak of quercetin (370 nm) over time were tested. As shown in Figure 2A, about 75% of free quercetin was decomposed

rapidly after dispersed in water for 5 h while quercetin in CuS@ZIF-8-QT NPs was degraded about 32%. However, only 20% quercetin of FA-BSA/CuS@ZIF-8-QT NPs was degraded. The variations of quercetin UV absorbance of quercetin in FA-BSA/CuS@ZIF-8-QT NPs over times in 36 h were illustrated in Figure 2B. The UV absorbance of quercetin decreased by around 36% in 36 h. These results verified that our drug delivery carriers with FA-BSA modification could significantly improve the stability of quercetin. In general, the instability of quercetin is mainly attributed to the oxidative decarboxylation of ring C.[40] While BSA is a good reductant due to tyrosine (Tyr) residues as investigated before.[41,42] Therefore, the BSA moiety in FA-BSA can inhibit oxidation degradation of quercetin. Moreover, the ZIF-8 can work as a protection layer for the loaded quercetin to weak its degradation. Consequently, the highest stability of quercetin in FA-BSA/CuS@ZIF-8-QT NPs was realized.

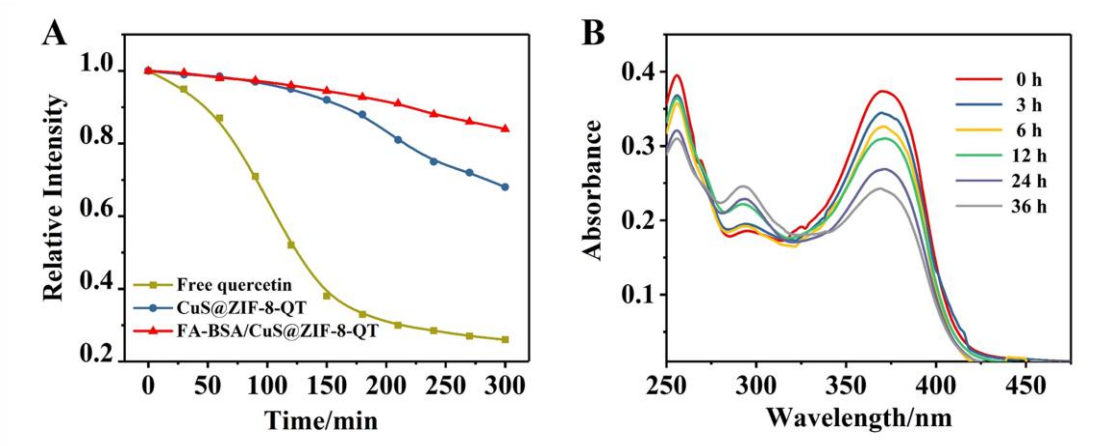


Figure 2. A) Relative intensity of the maximum UV absorbance of quercetin in different samples over time. B) The variations of quercetin UV absorbance in FA-BSA/CuS@ZIF-8-QT NPs aqueous solution over time in 36 h.

3.2. Photothermal Performance and *In Vitro* Drug Release of FA-BSA/CuS@ZIF-8-QT NPs. Firstly, the heat-generating capacity of the FA-BSA/CuS@ZIF-8-QT NPs solution was studied by measuring the temperature increase upon NIR laser exposure. As depicted in Figure 3A and Figure 3B, the heat-generating capacity of FA-BSA/CuS@ZIF-8-QT NPs was comparable to the capacity of CuS NPs. Then Figure 3C and Figure S4 revealed that FA-BSA/CuS@ZIF-8-QT NPs displayed irradiation time-, power intensity- and concentration-dependent photothermal effects and 2 W cm^{-2} was a suitable power intensity for in vitro studies. After exposing to 808 nm laser (2 W cm^{-2}) for 5 min, the temperature of FA-BSA/CuS@ZIF-8-QT NPs aqueous dispersion at the concentration of 100 μg mL^{-1} increased even by 34.5 °C. By contrast, pure ZIF-8 NPs solution only had negligible temperature increment at the same conditions. The above measurements suggested that FA-BSA/CuS@ZIF-8-QT exhibited satisfactory photothermal effect, demonstrating it could serve as a PTT agent for thermal ablation in tumor therapy.

After fully disintegrated in diluted hydrochloric acid (0.1 M), drug loading capacity of FA-BSA/CuS@ZIF-8-QT was determined using the method of UV spectrophotometry (Figure S5). The drug loading capacity of quercetin was determined to approximately 24%. Such high drug loading capacity is of great significance for the practical application of quercetin in cancer therapy since most of the reported anticancer drug loading capacity in carriers is only below 10%.

To evaluate the release behaviors of FA-BSA/CuS@ZIF-8-QT NPS, the cumulative

release profiles of quercetin in PBS at pH = 7.4 (imitates artificial physiological environment) and pH 5.0 (stimulates the acidic environment of endosome/lysosome), with or without NIR light irradiation were investigated. As shown in Figure 3D, without laser irradiation, quercetin was released in a pH dependent manner. Specifically, at pH 5.0 condition, the accumulative release amount of quercetin reached 45.0% after 48 h, meanwhile only 20.9% of quercetin had released at pH 7.4 condition. This pH-dependent manner is due to the protonation of the 2-methylimidazole linkers in the acidic condition, which breaks the coordination between zinc ions and imidazolate rings.[43] In addition, significant promotions of the quercetin releasing rate was monitored at both pH conditions after 5 min irradiation with 808 nm laser at 3 h. To be specific, the accumulated release ratio at pH 5.0 condition increased from 45.0% to 58.5% with the laser irradiation and a similar variation tendency was found at pH 7.4. It was worth mentioning that the drug release behaviors of pH 5.0 and pH 7.4 were similar in the initial stage with relatively fast release, which might be caused by the release of absorbed QT on the surface defects of ZIF-8 in the early time. These results demonstrated that the FA-BSA/CuS@ZIF-8-QT NPs had a pH-responsive and NIR-induced release behavior, which contributed to enhanced cytotoxicity toward tumor cells selectively.

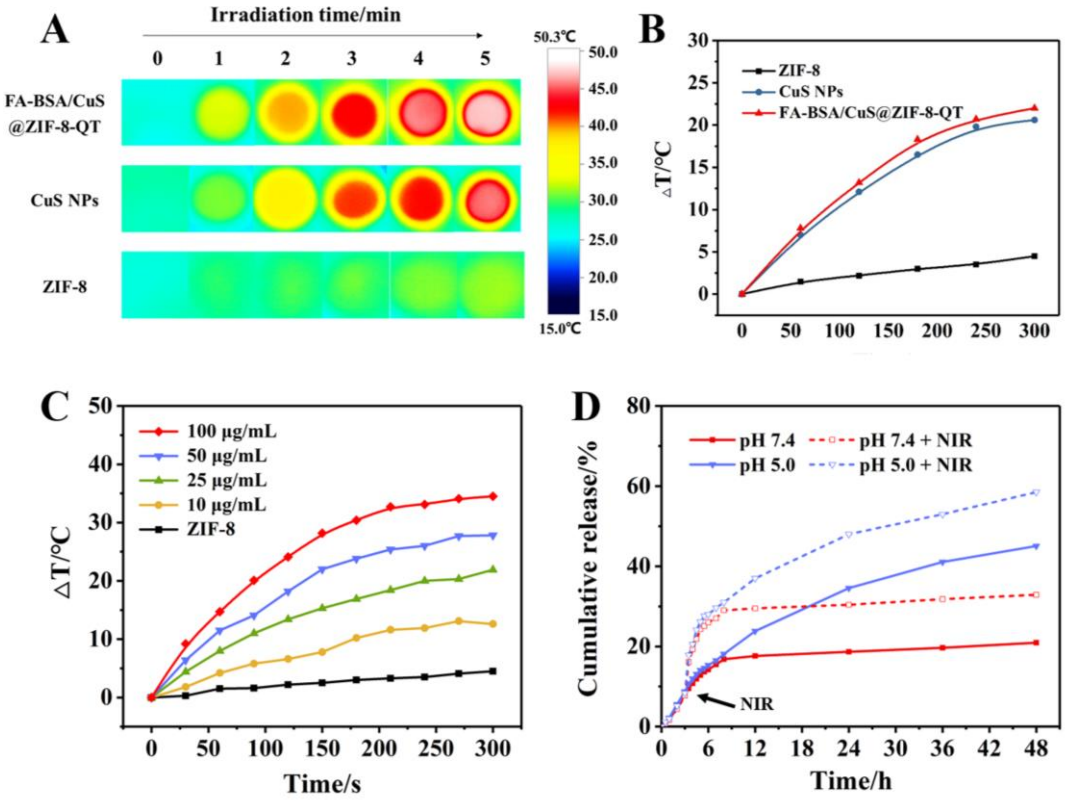


Figure 3. A, B) Infrared thermography and the corresponding temperature increase profiles of ZIF-8, CuS NPs, and FA-BSA/CuS@ZIF-8-QT (Cu^{2+} concentration = 0.5 mM) irradiated with 808 nm laser. C) Photothermal heating curves of pure ZIF-8 and different concentrations of FA-BSA/Cus@ZIF-8-QT by irradiation of an 808 nm laser. D) *In vitro* release of quercetin from FA-BSA/CuS@ZIF-8-QT NPs in PBS 7.4 and pH 5.0 with or without NIR (808 nm, 2 W cm^{-2}, 5 min).

3.3. Hemolysis Assay and *In Vitro* Cytotoxicity of FA-BSA/CuS@ZIF-8-QT NPs. Hemolysis assay was carried out to preliminary assess the biocompatibility and feasibility of FA-BSA/CuS@ZIF-8-QT NPs for intravenous administration. Figure 4A illustrated the hemolysis ratios of the FA-BSA/CuS@ZIF-8-QT in the range of experimental concentration (CuS concentration range: 1−200 μg mL^{-1}) were less than

5%, indicting good biocompatibility and safety of FA-BSA/CuS@ZIF-8-QT NPs for intravenous administration. It's worth mentioning that the hemolysis ratio of 200 μg mL^{-1} CuS NPs reached up to 26.4%, while the hemolysis ratios of CuS@ZIF-8 and CuS@ZIF-8-QT with the same CuS concentration are only 4.5% and 4.0% respectively, indicating that the hemolytic toxicity of CuS NPs drastically reduced when embedded in ZIF-8 matrix.

The *in vitro* cell growth inhibition rate with various treatments, including chemotherapy alone, PTT alone and combination of chemotherapy and PTT were investigated by MTT method. As shown in Figure 4B, the cytotoxicity of various treatment groups displayed dose-dependencies on the B16F10 cell lines. CuS@ZIF-8 without laser irradiation didn't cause significant cytotoxicity until at high concentration of CuS, suggesting the satisfactory biocompatibility of the carriers. However, CuS@ZIF-8 exhibited significant cytotoxicity under NIR irradiation, which was even better than FA-BSA/CuS@ZIF-8-QT at some conditions. The better inhibition effects of CuS@ZIF-8 + NIR could be ascribed to high efficiency of PTT and incomplete release of quercetin from FA-BSA/CuS@ZIF-8-QT (only about 30.4% in 24 h as shown in Figure 3D). The cell inhibition rate of CuS@ZIF-8-QT (quercetin concentration: 150 μM) under NIR irradiation can reached up to 80.3 ± 1.4%, significantly higher than that of free QT alone (48.1 ± 2.6%) or Cus@ZIF-8 with NIR irradiation (71.4 ± 5.2%). Thus, the combination of chemotherapy and PTT was superior to chemotherapy alone or PTT alone. According to the formula: $T_{add} = 1 - (f_{chemotherapy} \times f_{PTT})$, where T_{add} represents the additive therapeutic efficacy formula,

f is the cell viability of each treatment, [44-46] T_{add} of chemotherapy (free quercetin group, $f_{chemotherapy}$ = 51.9%) and PTT (FA-BSA/CuS@ZIF-8-QT group, f_{PTT} = 28.7%) was 85.1%, lower than combination of chemotherapy and PTT (93.3%, FA-BSA/CuS@ZIF-8-QT group + NIR group) at the concentration of 150 μM, demonstrating a synergistic effect for the combined therapy. Moreover, FA-BSA/Cus@ZIF-8-QT exhibited better therapeutic efficacy than CuS@ZIF-8-QT under NIR irradiation. For example, the cell inhibition rate of FA-BSA/Cus@ZIF-8-QT under NIR irradiation reached up to 93.3 ± 0.6% at the concentration of 150 μM, while the cell inhibition rate of CuS@ZIF-8-QT with NIR irradiation was 80.3 ± 1.4%. The higher therapy efficacy of FA-BSA/Cus@ZIF-8-QT could be attributed to enhanced cellular uptake of the targeted MOFs with FA-BSA modification.

In addition, flow cytometry assay was performed to quantitatively analyze cell apoptosis at each treatment group. The flow cytometry result was consistent with the above MTT results as shown in Figure 4C. The FA-BSA/CuS@ZIF-8-QT with NIR irradiation group shows the highest percentage of cell apoptosis (76.1%), much higher than that of FA-BSA/CuS@ZIF-8-QT (63.8%), Cus@ZIF-8 with NIR irradiation (59.5%) and CuS@ZIF-8-QT with NIR irradiation group (70.2%). The results above further proved the synergistic anticancer efficacy of quercetin and PTT.

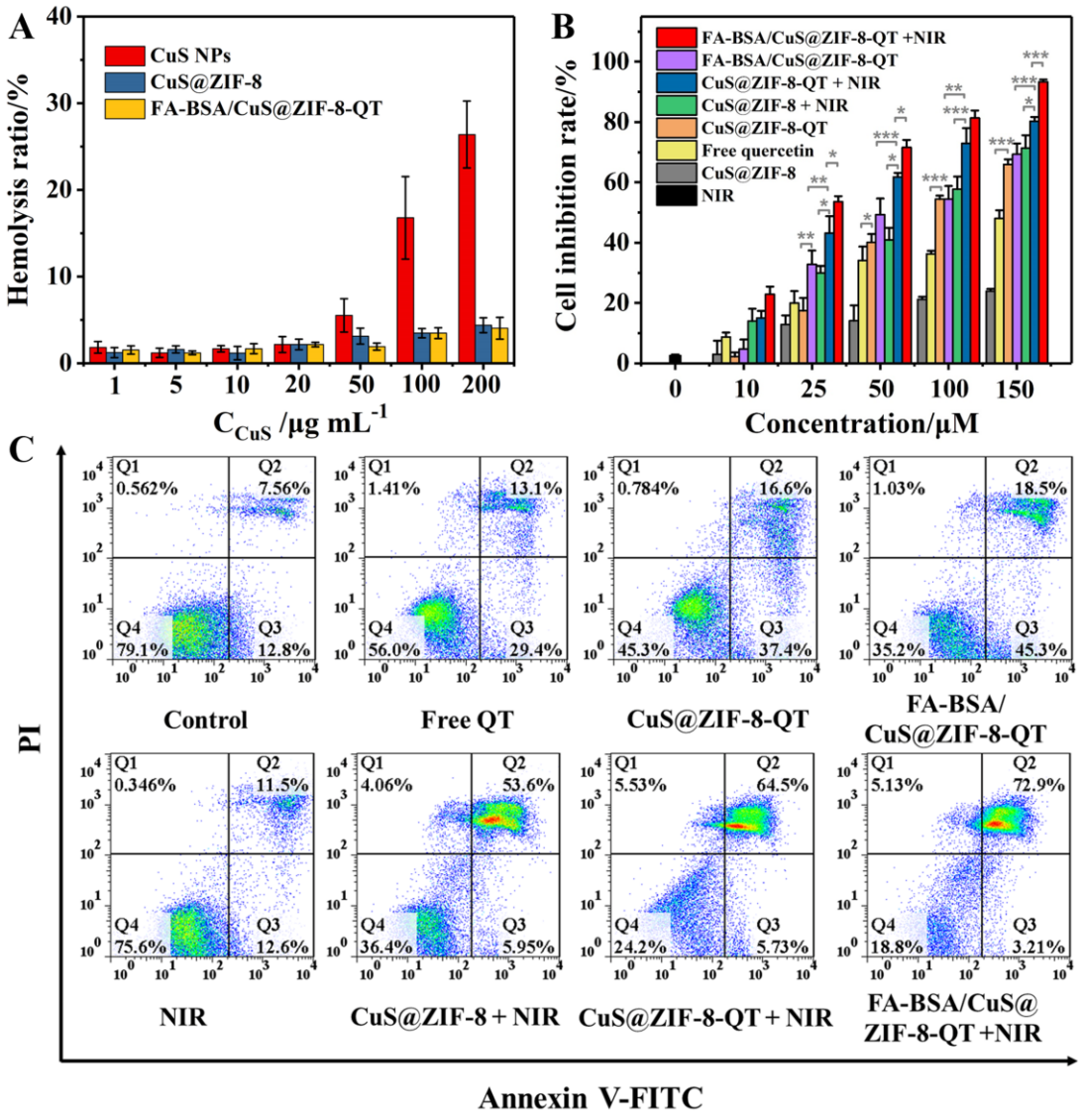


Figure 4. A) Hemolysis ratios of CuS NPs, CuS@ZIF-8 and FA-BSA/CuS@ZIF-8-QT at different concentrations. B) Cell inhibition rate after 24 h of incubated with various treatments. C) Flow cytometric analyses of apoptosis of B16F10 cells after different treatments. For NIR-related treatments, cells were exposed to 808 nm laser (2 W cm^{-2}, 5 min) after 4 h incubation of formulations. (*, $p < 0.05$; **, $p < 0.01$; ***, $p < 0.005$).

3.4. *In Vitro* Cellular Uptake Assay. FA-BSA/CuS@ZIF-8 NPs were labeled with

IR820 (fluorescent agent) to investigate their cellular uptake behavior. Fluorescence microscopy images of B16F10 treated with different formulations were presented in Figure 5A. When treated with free IR820, only weak fluorescence signals were observed, demonstrating the low uptake properties of IR820 alone. On the contrary, there were stronger fluorescence signals in the cells treated with CuS@ZIF-8-IR820, suggesting that nanoscale carriers could promote cellular uptake through endocytic pathway.[47, 48] Furthermore, the fluorescence intensity of FA-BSA/CuS@ZIF-8-IR820 group was obviously higher than that of CuS@ZIF-8-IR820. The result indicated that FA-BSA/CuS@ZIF-8-IR820 exhibited remarkable more efficient cellular uptake behavior, which would be ascribed to the targeting effect of the folate to overexpressed FA-receptors (FR) on the tumor cells. The quantitative results obtained by flow cytometry were in accordance with the qualitative results of fluorescence microscopic images as shown in Figure 3. The cells treated with nanoparticles showed remarkably more drug accumulations than free IR820 and the cellular uptake of all the formulations were in order of FA-BSA/CuS@ZIF-8-IR820 > CuS@ZIF-8-IR820 > free IR820 in B16F10 cells. The results further confirmed that FA-BSA modification can effectively enhance the cellular uptake through FR-mediated endocytosis.

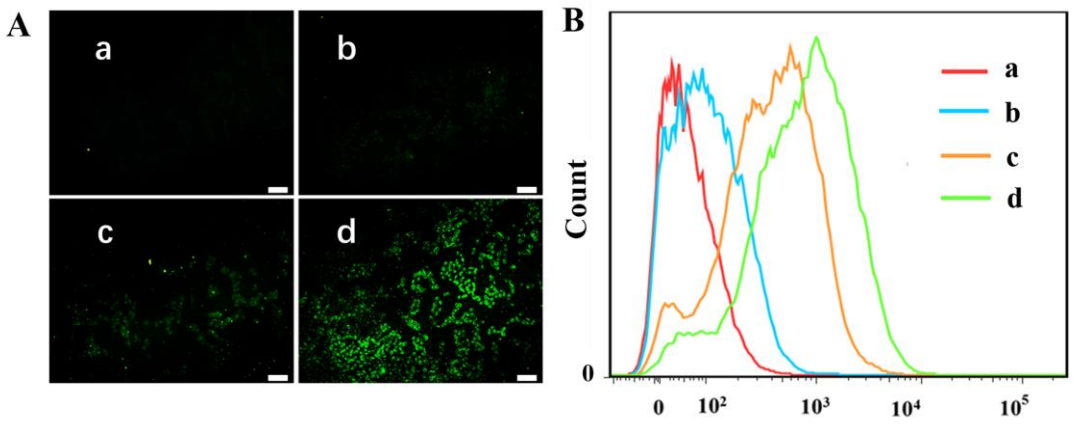


Figure 5. A) Fluorescence microscopic images and B) fluorescence intensity of B16F10 cells incubated with (a) blank, (b) free IR820, (c) CuS@ZIF-8-IR820 and (d) FA-BSA/CuS@ZIF-8-IR820 for 4 h, (C_{IR820} = 20 μg mL^{-1}). The scale bar is 100 μm.

3.5. *In Vivo* NIRF Imaging. Before investigating the anti-tumor efficacy, the biodistribution studies of FA-BSA/CuS@ZIF-8 NPs were carried out to investigated the *in vivo* targeted behavior of FA-BSA/CuS@ZIF-8 NPs. Here, IR820 labeled FA-BSA/CuS@ZIF-8 was used as the studied system since IR820 is an excellent fluorescence marker for *in vivo* imaging. In short, tumor bearing mice were intravenously injected with CuS@ZIF-8-IR820 or FA-BSA/CuS@ZIF-8-IR820, then monitored by a near infrared optical imaging technique. Figure. 6A showed the fluorescent images of mice at 1, 2, 4, 6, 8, 12, 24 h postinjection. Compared with CuS@ZIF-8-IR820 group, stronger fluorescence signals could be observed at the tumor sites of FA-BSA/CuS@ZIF-8-IR820 group throughout the experiment. These results demonstrated more accumulation of FA-BSA/CuS@ZIF-8-IR820 NPs at the tumor site, which was ascribed to the folate mediated active targeting effect. The fluorescent intensity on the tumor areas of both groups reached to the highest at 8 h

postinjection, then decreased gradually, suggesting this moment was the optimal time to give laser. In addition, the fluorescence in the tumor of FA-BSA/CuS@ZIF-8-IR820 group (fluorescence intensity: 3.16E+06 a. u.) was significantly stronger than that of CuS@ZIF-8-IR820 group (fluorescence intensity: 1.32E+06 a. u.) at 8 h postinjection (Table S1), indicting satisfactory targeting ability of FA-BSA/CuS@ZIF-8-IR820. Furthermore, the main organs and tumors were excised for measurements of their fluorescence intensity at 24 h postinjection. As illustrated in Figure 6B and Table S2, the fluorescence in the tumor of FA-BSA/CuS@ZIF-8-IR820 group (fluorescence intensity: 1.20E+06 a. u.) was significantly stronger than that of CuS@ZIF-8-IR820 group (fluorescence intensity: 7.06E+05 a. u.). Notably, only weak fluorescence signals could be observed in the spleens and hearts of both groups, suggesting little side effects to spleen and heart. These results indicated that FA-BSA/CuS@ZIF-8 NPs could efficiently accumulate into the tumor site via folate mediated active targeting effect besides the EPR effect, thus maximizing anti-tumor effects as well as minimizing side effects.

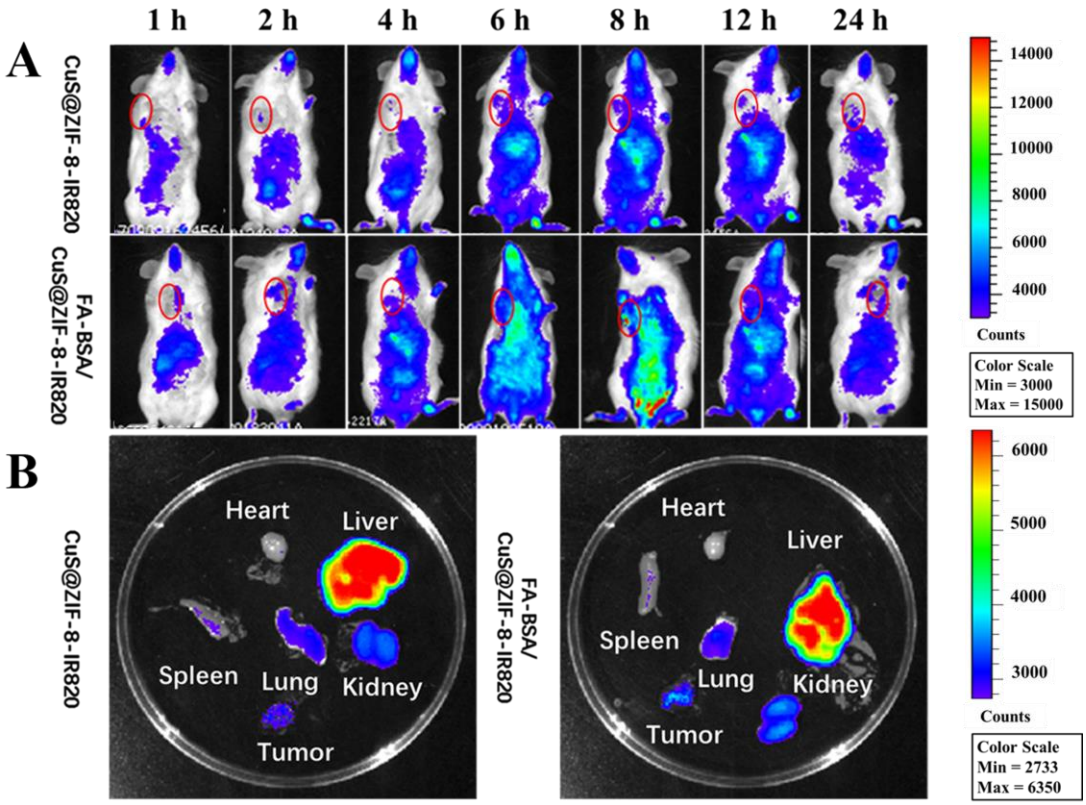


Figure 6. A) *In vivo* NIRF imaging and biodistribution of CuS@ZIF-8-IR820 and FA-BSA/CuS@ZIF-8-IR820 at various time points after the injection. Tumor site was marked with red ellipse. B) Fluorescence photographs of tumors and main organs at 24 hours after injection of CuS@ZIF-8-IR820 and FA-BSA/CuS@ZIF-8-IR820.

3.6. *In Vivo* Infrared Thermography and Anti-Tumor Efficacy Assay. The *in vivo* photothermal performance and anti-tumor effect of FA-BSA/CuS@ZIF-8-QT were evaluated by four groups of B16F10 tumor bearing mice. Temperature change of the tumor region during irradiation of 808 nm laser after administration was recorded by a thermal camera and the results were presented in Figure 7A. Only several degrees temperature increase was observed at the tumor site for mice injected with saline. In contrast, the temperature of FA-BSA/CuS@ZIF-8-QT group and

CuS@ZIF-8-QT group could increase to 58 °C and 54 °C respectively, meeting requirements for PTT.[49-51] Figure 7B showed the representative photos of B16F10 tumor-bearing mice in various treatment groups and the excised tumors from each group at the end of treatments. Figure 7C showed the relative tumor volumes (V/V_0) changes after various treatments during the treatment. Compared with control group (NS + NIR), free quercetin + NIR group exhibited no significant anti-tumor efficacy, which was attributed to the instability and poor solubility of pure quercetin. On the contrary, FA-BSA/CuS@ZIF-8-QT + NIR group and CuS@ZIF-8-QT group exhibited remarkable anti-tumor efficacy and the former one was much better, indicating excellent therapeutic effect of combined chemotherapy and PTT as well as superiority of active targeting. As shown in Figure 7D, tumor inhibition ratio of FA-BSA/CuS@ZIF-8-QT + NIR group was the highest, up to 91.8 ± 5.1%, further demonstrating the best therapeutic effect of this treatment. The survival rate of the FA-BSA/CuS@ZIF-8-QT + NIR group was significantly higher than control group, also demonstrating the good efficacy and safety of this treatment (Figure S6). The body weight changes of the mice were illustrated in Figure 7E, from which no significant difference was observed, indicating that the FA-BSA/CuS@ZIF-8-QT NPs had little side effect.

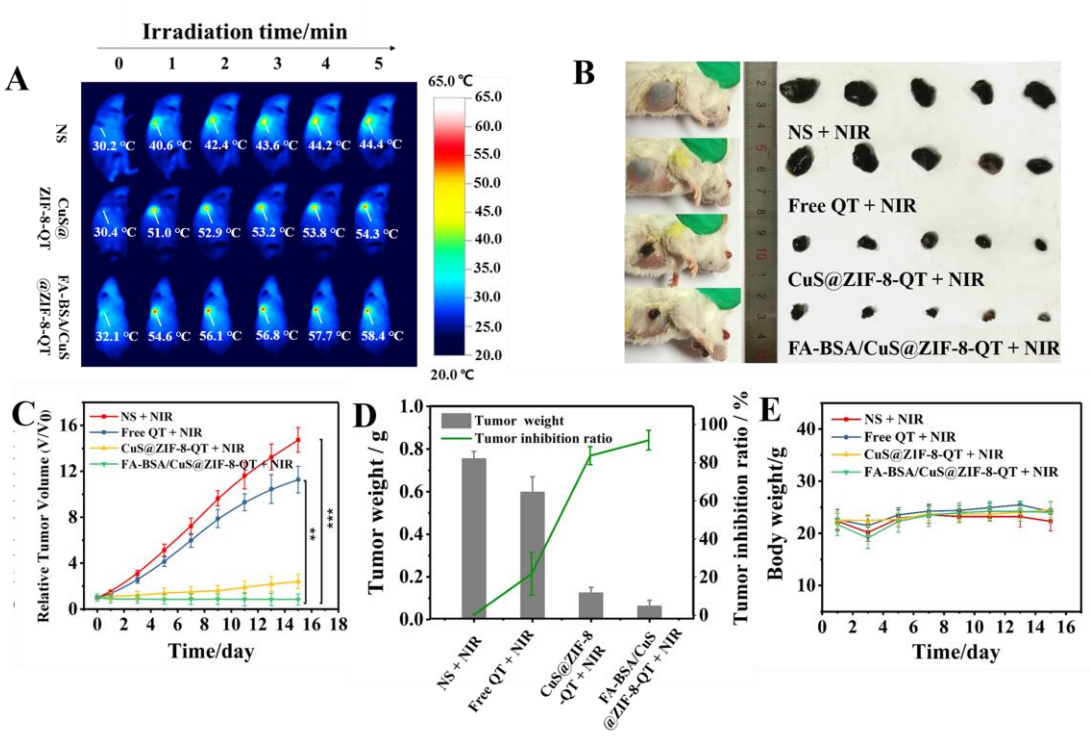


Figure 7. A) Infrared thermography of B16F10 tumor bearing mice with irradiation of 808 nm laser (1 W cm^{-2}) at 8 h after injection with NS, CuS@ZIF-8-QT or FA-BSA/CuS@ZIF-8-QT. B) Photos of the mice after different treatments and the tumors dissected from each group at the end of treatments. C) Tumor volume changes, D) tumor weight and tumor inhibition ratio and E) changes in body weight of mice with various treatments within 15 d. (*, $p < 0.05$; **, $p < 0.01$; ***, $p < 0.005$).

3.7. Histology Analysis. To further evaluate the safety and anti-tumor efficacy of FA-BSA/CuS@ZIF-8-QT, mice were dissected after the anti-tumor efficacy assay. Tumors and main organs were harvested for histological analysis. The histology analysis results of the tumors and major organs of each group were shown in Figure 8. Different degrees of tumor damage characterized by cell shrinkage as well as nuclear chromatin condensation and fragmentation were observed in various treatment groups. Among the various treatments, most severe tumor damage was found in the

FA-BSA/CuS@ZIF-8-QT + NIR group, demonstrating that the FA-BSA/CuS@ZIF-8-QT + NIR group has the best anti-tumor effect. In addition, comparing with control group, no significant abnormality was found in the major organ sections of all treatment groups, indicating that all treatments didn't cause significant toxicity to major organs. All the above results demonstrate that FA-BSA/CuS@ZIF-8-QT exhibit satisfactory safety to normal organs and excellent antitumor efficacy through combined PTT and chemotherapy.

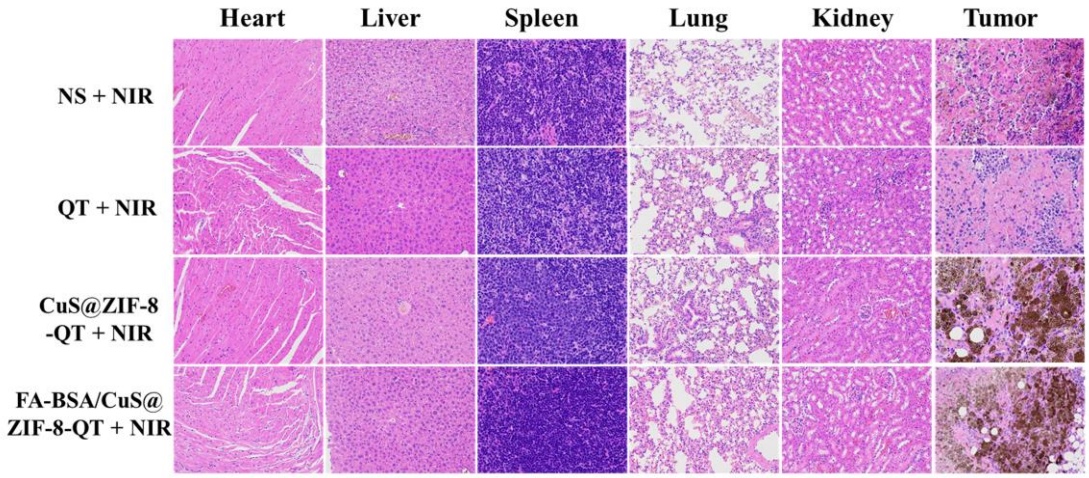


Figure 8. Hematoxylin and eosin (HE)-stained images of main organs and tumors of tumor bearing mice with various treatments.

4. Conclusions

In summary, a combinational therapy platform of quercetin as anticancer agent without side effect and CuS NPs as PTT agent based on FA-BSA modified ZIF-8 was constructed for the first time. Our designed FA-BSA/CuS@ZIF-8-QT exhibited uniform spherical morphology with suitable size, high drug loading contents of quercetin with the pH-responsive and NIR-induced release behavior. In particular, the

drawbacks of poor bioavailability, low water-solubility and chemical instability of quercetin are sufficiently overcome by our smart designed FA-BSA/CuS@ZIF-8 as the drug delivery system. The stability study demonstrates that chemical stability of quercetin is improved largely with the application of FA-BSA/CuS@ZIF-8 as drug carrier. *In vitro* cellular uptake and *in vivo* NIRF imaging results demonstrate that FA-BSA-modified MOF remarkably enhancing cellular uptake of tumor cells both *in vivo* and *in vitro*. The FA-BSA/CuS@ZIF-8-QT shows negligible toxicity and low hemolysis ratio to normal organs, which demonstrates that it is safe to administered intravenously. The anticancer experimental results *in vivo* and *in vitro* indicated that the FA-BSA/CuS@ZIF-8-QT with NIR irradiation treatment had distinctly superior anticancer effect over the chemotherapy or PTT alone, with significantly enhanced the tumor growth inhibition. Consequently, our designed pH-resposive and tumor-targeted drug delivery system successfully solves the drawback of quercetin, which offers a promising nanoplatform for the application of quercetin in cancer therapy.

ASSOCIATED CONTENT

Supporting Information

UV-Vis absorbance spectra of FA, BSA and FA-BSA. The obvious absorbance at 347 nm of FA-BSA spectrum proved the successful synthesis of FA-BSA (Figure S1) SEM image and elemental mapping images of CuS@ZIF-8 particles (Figure S2); Zeta potentials of ZIF-8, CuS@ZIF-8, CuS@ZIF-8-QT and FA-BSA/CuS@ZIF-8-QT

(Figure S3); photothermal heating curves of FA-BSA/Cus@ZIF-8-QT (150 μM) by irradiation with 808 nm laser at various power intensities(Figure S4); UV–vis absorbance spectra of CuS@ZIF-8 and CuS@ZIF-8-QT dissolved in methanol after fully disintegrated in diluted hydrochloric acid (0.1 M) (Figure S5); the survival rate curves of tumor bearing mice with various treatments (Figure S6); mean fluorescence intensities of tumors areas after injection of CuS@ZIF-8-IR820 and FA-BSA/CuS@ZIF-8-IR820 at various time points after the injection (Table S1); mean fluorescence intensities of tumors and major organs after injection of CuS@ZIF-8-IR820 and FA-BSA/CuS@ZIF-8-IR820 at 24 h (Table S2).

AUTHOR INFORMATION

Corresponding Authors

*E-mail: yuxialuan@sdu.edu.cn. Tel: (86) 531-88382007. Fax: (86) 531-88382548.

Notes

The authors declare no competing financial interest.

ACKNOWLEDGEMENTS

This work was supported by the National Natural Science Foundation of China (NSFC, No. 21872083 and No. 21673128), Shandong Provincial Major Science & Technology Innovation Project (2018CXGC1411), The Fundamental Research Funds of Shandong University (2018JC019) and the China-Australia Centre for Health Science Research (CACHSR).

References

(1) Ahmedin, J.; Freddie, B.; Melissa, M. C.; Jacques, F.; Elizabeth, W.; David, F. Global Cancer Statistics. *CA Cancer J. Clin.* **2011**, 61, 69-90.

(2) Rebecca, L. S.; Kimberly, D. M.; Ahmedin, J. Cancer Statistics, 2015. *CA Cancer J. Clin.* **2015**, *65*, 5-29.

(3) Ravishankar, D.; Rajora, A. K.; Greco, F.; Osboarn, H. M. I. Flavonoids as Prospective Compounds for Anti-Cancer Therapy. *Int. J. Biochem. Cell B* **2013**, *45*, 2821-2831.

(4) Bischoff; Stephan, C. Quercetin: Potentials in the Prevention and Therapy of Disease. *Curr. Opin. Clin. Nutr. Metab. Care* **2008**, *11*, 733-740

(5) Wang, W. Y.; Sun, C. X.; Mao, L.; Ma, P. H.; Liu, F. G.; Yang, J.; Gao, Y. X. The Biological Activities, Chemical Stability, Metabolism and Delivery Systems of Quercetin: A Review. *Trends Food Sci. Tech.* **2016**, *58*, 21-38.

(6) Chang, J. H.; Lai, S. L.; Chen, W. S.; Hung, W. Y.; Chow, J. M.; Hsiao, M.; Lee, W. J.; Chien, M. H. Quercetin Suppresses the Metastatic Ability of Lung Cancer Through Inhibiting Snail-Dependent Akt Activation and Snail-Independent ADAM9 Expression Pathways. *BBA-Mol. Cell Res.* **2017**, *1864*, 1746-1758.

(7) Srivastava, S.; Somasagara, R.R.; Hegde, M.; Nishana, M.; Tadi, S. K.; Srivastava, M.; Choudhary, B.; Raghavan, S. C. Quercetin, a Natural Flavonoid Interacts with DNA, Arrests Cell Cycle and Causes Tumor Regression by Activating Mitochondrial Pathway of Apoptosis. *Sci. Rep.* **2016**, *6*, 24049-24062.

(8) Harwood, M.; Danielewska-Nikiel, B.; Borzelleca, J. F.; Flamm, G. W.; Williams, G. M.; Lines, T. C. A Critical Review of the Data Related to the Safety of

Quercetin and Lack of Evidence of *In Vivo* Toxicity, Including Lack of Genotoxic/Carcino Genic Properties. *Food Chem. Toxicol.* **2007**, *45*, 2179-2205.

(9) Utesch, D.; Feige, K.; Dasenbrock, J.; Broschard, J. H.; Harwood, M.; Danielewska-Nikiel, B.; Lines, T. C. Evaluation of the Potential *In Vivo* Genotoxicity of Quercetin. *Mutat. Res.* **2008**, *654*, 38-43.

(10) Bonferoni, M. C.; Rossi, S.; Sandri, G.; Ferrari, F. Nanoparticle formulations to Enhance Tumor Targeting of Poorly Soluble Polyphenols with Potential anticancer Properties. *Semin. Cancer Biol.* **2017**, *46*, 205-214

(11) Ratnam, D. V.; Ankola, D. D.; Bhardwaj, V.; Sahana, D. K.; Kumar, M. N. Role of Antioxidants in Prophylaxis and Therapy: A Pharmaceutical Perspective. *J. Control. Release* **2006**, *113*, 189-207

(12) Horcajada, P.; Serre, C.; Maurin, G.; Ramsahye, N. A.; Balas, F.; Vallet-Regí, M.; Sebban, M.; Taulelle, F.; Ferey, G. Flexible Porous´ Metal-Organic Frameworks for a Controlled Drug Delivery. *J. Am. Chem. Soc.* **2008**, *130*, 6774-6780.

(13) Chen, B.; Yang, Z.; Zhu Y.; Xia, Y. Zeolitic Imidazolate Framework Materials: Recent Progress in Synthesis and Applications. *J. Mater. Chem. A* **2014**, *2*, 16811 -16831.

(14) Sun, C. Y.; Qin, C.; Wang, C. G.; Su, Z. M.; Wang, S.; Wang, X. L.; Yang, G. S.; Shao, K. Z.; Lan, Y. Q.; Wang, E. B. Chiral Nanoporous Metal-Organic Frameworks with High Porosity as Materials for Drug Delivery. *Adv. Mater.* **2011**, *23*, 5629-5632.

(15) Venna, S. R.; Jasinski J. B.; Carreon, M. A. Structural Evolution of Zeolitic

Imidazolate Framework-8. *J. Am. Chem. Soc.* **2010**, *132*, 18030-18033.

(16) Sun, C. Y.; Qin, C.; Wang, X. L.; Yang, G. S.; Shao, K. Z.; Lan, Y. Q.; Su, Z. M.; Huang, P.; Wang, C. G.; Wang, E. B. Zeolitic imidazolate framework-8 as Efficient pH-Sensitive Drug Delivery Vehicle. *Dalton Trans.* **2012**, *41*, 6906-6909.

(17) Zhang, H. Y.; Jiang, W.; Liu, R. L.; Zhang, J.; Zhang, D.; Li, Z. H.; Luan, Y. X. Rational Design of Metal Organic Framework Nanocarrier-Based Codelivery System of Doxorubicin Hydrochloride/Verapamil Hydrochloride for Overcoming Multidrug Resistance with Efficient Targeted Cancer Therapy. *ACS Appl. Mater. Interfaces* **2017**, *9*, 19687-19697.

(18) Li, X.; Shan, J. Y.; Zhang, W. Z.; Su, S.; Yuwen, L. H.; Wang. L. H. Recent Advances in Synthesis and Biomedical Applications of Two-Dimensional Transition Metal Dichalcogenide Nanosheets. *Small* **2017**, *13*, 1602660.

(19) Chen, Q.; Wen, J.; Li, H.; Xu, Y. Dual Roles of Protein as a Template and a Sulfur Provider: A General Approach to Metal Sulfides for Efficient Photothermal Therapy of Cancer. *Small* **2018**, *14*, 1702529.

(20) Liang, C.; Xu, L. G.; Song, G. S.; Liu, Z. Emerging Nanomedicine Approaches Fighting Tumor Metastasis: Animal Models, Metastasis-Targeted Drug delivery, Phototherapy, and Immunotherapy. *Chem. Soc. Rev.* **2016**, *45*, 6250-6269.

(21) Tian, Z. F.; Yao, X. X.; Ma, K. X.; Niu, X. X.; Grothe, J; Xu, Q. N.; Liu, L. S.; Kaskel, S.; Zhu, Y. F. Metal−Organic Framework/Graphene Quantum Dot Nanoparticles Used for Synergistic Chemo- and Photothermal Therapy. *ACS*

Omega **2017**, *2*, 1249−1258.

(22) Tian, Z. F.; Yao, X. X.; Zhu, Y. F. Simple Synthesis of Multifunctional Zeolitic Imidazolate Frameworks-8/Graphene Oxide Nanocrystals with Controlled Drug Release and Photothermal Effect. *Micropor. Mesopor. Mat.* **2017**, *237*, 160-167.

(23) Yao, X. X.; Niu, X. X.; Ma, K. X.; Huang, P.; Grothe, J.; Kaskel, S.; Zhu, Y. F. Graphene Quantum Dots-Capped Magnetic Mesoporous Silica Nanoparticles as a Multifunctional Platform for Controlled Drug Delivery, Magnetic Hyperthermia, and Photothermal Therapy. *Small* **2017**, *13*, 1602225.

(24) Yao, X. X.; Tian, Z. F.; Liu, J. X.; Zhu, Y. F.; Hanagata, N. Mesoporous Silica Nanoparticles Capped with Graphene Quantum Dots for Potential Chemo-Photothermal Synergistic Cancer Therapy. *Langmuir* **2017**, *33*, 591−599.

(25) Wang, Y. Y.; Liu, X. J.; Deng, G. Y.; Sun, J.; Yuan, H. K.; Li, Q.; Wang, Q. G.; Lu, J. Se@SiO_2-FA-CuS Nanocomposites for Targeted Delivery of DOX and Nano Selenium in Synergistic Combination of Chemo-Photothermal Therapy. *Nanoscale* **2018**, *10*, 2866–2875.

(26) Wang, Y. Y.; Liu, X. J.; Deng, G. Y.; Wang, Q.; Zhang, L. J.; Wang, Q. G.; Lu, J. Multifunctional PS@CS@Au-Fe_3O_4-FA nanocomposites for CT, MR and fluorescence imaging guided targeted-photothermal therapy of cancer cells. *J. Mater. Chem. B* **2017**, *5*, 4221—4232.

(27) Ren, L. F.; Liu, X. J.; Wang, Q.; Zhang, L. J.; Deng, G. Y.; Zhou, F.; Lu, J. Facile Fabrication of a Magnetically Smart PTX-Loaded Cys-Fe_3O_4/CuS@BSA Nano-Drug for Imaging-Guided Chemo-Photothermal Therapy. *Dalton Trans.*

2017, *46*, 2204–2213.

(28) Gao, Z. F.; Liu, X. J.; Deng, G. Y.; Zhou, F.; Zhang, L. J.; Wang, Q.; Lu, J. Fe_3O_4@mSiO_2-FA-CuS-PEG Nanocomposites for Magnetic Resonance Imaging and Targeted Chemo-Photothermal Synergistic Therapy of Cancer Cells. *Dalton Trans.* **2016**, *45*, 13456–13465.

(29) Wang, Z. F.; Tang, X. J.; Wang, X. X.; Yang, D. D.; Yang, C.; Lou, Y. B.; Chen, J. X.; He, N. Y. Near-Infrared Light-Induced Dissociation of Zeolitic Imidazole Framework-8 (ZIF-8) with Encapsulated CuS Nanoparticles and Their Application as a Therapeutic Nanoplatform. *Chem. Commun.* **2016**, *52*, 12210-12213.

(30) Liu, J. B.; Fu, S. H.; Yuan, B.; Li, Y. L.; Deng, Z. X. Toward a Universal "Adhesive Nanosheet" for the Assembly of Multiple Nanoparticles Based on a Protein-Induced Reduction/Decoration of Graphene Oxide. *J. Am. Chem. Soc.* **2010**, *132*, 7279-7281.

(31) Hao, R. F.; Wu, X.; Li, Q.; Leng, X. J.; Jing, H. Bovine Serum Albumin Nanoparticle Promotes the Stability of Quercetin in Simulated Intestinal Fluid. *J. Agr. Food Chem.* **2011**, *59*, 6292-6298.

(32) Dufour, C.; Dangles, O. Flavonoid Serum Albumin Complexation: Determination of Binding Constants and Binding Sites by Fluorescence Spectroscopy. *Biochim. Biophys. Acta* **2005**, *1721*, 164-173.

(33) Ni, Y.; Zhang, X.; Kokot, S. Spectrometric and Voltammetric Studies of the Interaction between Quercetin and Bovine Serum Albumin using Warfarin as

Site Marker with the Aid of Chemometrics. *Spectrochim. Acta A: Mol. Biomol. Spectrosc.* **2009**, *71*, 1865-1872.

(34) Wang, Y.; Wang, X. Binding, Stability, and Antioxidant Activity of Quercetin with Soy Protein Isolate Particles. *Food Chem.* **2015**, *188*, 24-29.

(35) Liu, J.; Zhao, D. J.; He, W. X.; Zhang, H. Y.; Li, Z. H.; Luan, Y. X. Nanoassemblies from Amphiphilic Cytarabine Prodrug for Leukemia Targeted Therapy. *J. Colloid Interf. Sci.* **2017**, *487*, 239-249.

(36) Ma, N. X.; Liu, J.; He, W. X.; Li, Z. H.; Luan, Y. X.; Song, Y. M.; Garg, S. J. Folic Acid-Grafted Bovine Serum Albumin Decorated Graphene Oxide: An Efficient Drug Carrier for Targeted Cancer Therapy. *J. Colloid Interf. Sci.* **2017**, *490*, 598–607.

(37) Srinivasan, S.; Manchanda, R.; Fernandez-Fernandez, A.; Lei, T.; Mcgoron, A. J. Near-Infrared Fluorescing IR820-Chitosan Conjugate for Multifunctional Cancer Theranostic Applications. *J. Photochem. Photobiol. B* **2013**, *119*, 52-59.

(38) Fernandez-Fernandez, A.; Manchanda, R.; Lei, T.; Carvajal, D. A.; Tang, Y.; Kazmi, S. Z. R.; McGoron, A. J. Comparative Study of the Optical and Heat Generation Properties of IR820 and Indocyanine Green. *Mol. Imaging* **2012**, *11*, 99-113.

(39) Chen, Y.; Zheng, X. L.; Fang, D. L.; Yang, Y.; Zhang, J. K.; Li, H. L.; Xu, B.; Lei, Y.; Ren, K.; Song, X. R. Dual Agent Loaded PLGA Nanoparticles Enhanced Antitumor Activity in a Multidrug-Resistant Breast Tumor Eenograft Model. *Int. J. Mol. Sci.* **2014**, *15*, 2761-2772.

(40) Zenkevich, I. G.; Eshchenko, A. Y.; Makarova, S. V.; Vitenberg, A. G.; Dobryakov, Y. G.; Utsal, V. A. Identification of the products of oxidation of quercetin by air oxygen at ambient temperature. *Molecules* **2007**, *12*, 654-672.

(41) Xie, J. P.; Zheng, Y. G.; Ying, J. Y. Protein-Directed Synthesis of Highly Fluorescent Gold Nanoclusters. *J. Am. Chem. Soc.* **2009**, *131*, 888-889.

(42) Singh, A. V.; Batuwangala, M.; Mundra, R.; Mehta, K.; Patke, S.; Falletta, E.; Patil, R.; Gade, W.N. Biomineralized Anisotropic Gold Microplate–Macrophage Interactions Reveal Frustrated Phagocytosis-Like Phenomenon: A Novel Paclitaxel Drug Delivery Vehicle. *ACS Appl. Mater. Interfaces* **2014**, *6*, 14679-14689.

(43) Avci, C.; Arinez-Soriano, J.; Carne-Sanchez, A.; Guillerm, V.; Carbonell, C.; Imaz, I.; Maspoch, D. Post-Synthetic Anisotropic Wet-Chemical Etching of Colloidal Sodalite ZIF Crystals. *Angew. Chem. Int. Ed.* **2015**, *54*, 14417-14421.

(44) Ma, M.; Chen, H.; Chen, Y.; Wang, X.; Chen, F.; Cui, X.; Shi, J. Au Capped Magnetic Core/Mesoporous Silica Shell Nanoparticles for Combined Photothermo-/Chemo-Therapy and Multimodal Imaging. *Biomaterials* **2012**, *33*, 989-998.

(45) Park, H.; Yang, J.; Lee, J.; Haam, S.; Choi, I. H.; Yoo, K. H. Multifunctional Nanoparticles for Combined Doxorubicin and Photothermal Treatments. *ACS Nano* **2009**, *3*, 2919-2926.

(46) Hahn, G. M.; Braun, J.; Har-Kedar, I. Thermochemotherapy: Synergism Between Hyperthermia (42−43 degrees) and Adriamycin (of bloom's) in Mammalian Cell Inactivation. *Proc. Natl. Acad. Sci. U.S.A.* **1975**, *72*, 937-940.

(47) Chen, G. J.; Ma, B.; Wang, Y. Y.; Xie, R. S.; Li, C.; Dou K. F.; Gong, S. Q. CuS-based Theranostic Micelles for NIR-controlled Combination Chemotherapy and Photothermal Therapy and Photoacoustic Imaging. *ACS Appl. Mater. Interfaces* **2017**, *9*, 41700-41711.

(48) Bildstein, L.; Dubernet, C.; Couvreur, P. Prodrug-Based Intracellular Delivery of Anticancer Agents. *Adv. Drug Delivery Rev.* **2011**, *63*, 3-23.

(49) Jaque, D.; Maestro, L. M.; del Rosal, B.; Haro-Gonzalez, P.; Benayas, A.; Plaza, J. L.; Rodriguez, E. M.; Sole, J. G. Nanoparticles for Photothermal Therapies. *Nanoscale* **2014**, *6*, 9494-9530.

(50) Chakravarty, P.; Marches, R.; Zimmerman, N. S.; Swafford, A. D.; Bajaj, P.; Musselman, I. H.; Pantano, P.; Draper R. K.; Vitetta. E. S. Thermal Ablation of Tumor Cells with Antibody-Functionalized Single-Walled Carbon Nanotubes. *Proc. Natl. Acad. Sci. U. S. A.* **2008**, *105*, 8697-8702.

(51) Torti, S. V.; Byrne, F.; Whelan, O.; Levi, N.; Ucer, B.; Schmid, M.; Torti, F. M.; Akman, S.; Liu, J.; Ajayan, P. M.; Nalamasu, O.; Carroll, D. L. Thermal Ablation Therapeutics Based on CNx Multi-Walled Nanotubes. *Int. J. Nanomed.* **2007**, *2*, 707-714.

Table of Contents

